

FINAL
11/11/89
0.117
46151*Final Report***Investigation of Carbon Fiber Surface and Interface with Polyimide by Scanning Tunneling Microscopy (STM) and Computer Modeling***Grant #NAG3-1289*

R.K. Eby
The University of Akron
Department of Polymer Science
Akron, OH 44325-3909
(330) 972-7539

ABSTRACT

The goal of this work was to develop an understanding of the interfacial bonding in carbon fiber/PMR-15 polyimide composites. This understanding would provide a basis for interfacial tailoring to improve the bond strength and the thermo-oxidative stability of the composite. A variety of methods were used to characterize the bond strength, the thermo-oxidative stability, the polar nature of the surface of the carbon fibers, and the fine-scale structure/morphology of the fibers. Some of the work was carried out collaboratively with NASA Lewis researchers and some NASA Lewis facilities were used on occasion. The results show that the interfacial bonding is primarily dipolar between dipoles in the matrix and dipoles on the fiber surface. The concentration of the latter has been measured and the interlaminar shear strength (ILSS) has been shown to be linearly proportional to the increase of the polar concentration on the surface. This suggests the possibility of a limiting value of ILSS associated with dipoles. The mass loss and the decrease of bonding with time of aging in air at 316° C decrease with increasing concentration of dipoles on the surface. The nature of the fiber surface has been characterized qualitatively and quantitatively. The results indicate that the morphological features containing the bonding sites for the polar groups are at dimensional scales less than 25 nm. Some of these sites have been identified by AFM and STM at this scale as well as at the scale of atomic-resolution. Details of these and many other observations are given in the attached reports.

AFM Studies of PAN-based Carbon Fiber Surfaces: Interfacial Bonding with PMR-15 Polyimide

ITTIPOL JANGCHUD, A.M. SERRANO*, M.A. MEADOR** and R.K. EBY

Department and Institute of Polymer Science, The University of Akron, Akron, OH 44325, USA

**NASA Graduate Student Researcher Program Fellow at Lewis Research Center ; Present address:*

Dept. of Chemical Engineering, Cleveland State University, Cleveland, OH 44135 USA

***Polymer Branch, NASA Lewis Research Center, Cleveland, OH 44135, USA*

Corresponding author : *Ittipol Jangchud*

Department and Institute of Polymer Science

The University of Akron, Akron, OH 44325-3909

Tel : (330) 972-8282 FAX : (330) 972-6581

E-mail address : ittipol@eby.polymer.uakron.edu

Abstract- Atomic force microscopy (AFM) has been used to study the surfaces of a series of PAN-based carbon fibers in order to gain a better understanding of their interfacial interactions with PMR-15 polyimide. Digitized AFM data yield surface topographic images together with surface parameters, such as, average roughness (R_a), area (A_c), and fractal dimension (F_d). The results show that the correlation between dipole components on the surface and the initial interlaminar shear strength (ILSS) of the composites is quadratic. Previous [1] correlations of roughness with dipole components on the fiber surfaces as well as, therefore, with the ILSS of the composites are not as satisfactory when extended to additional types of fibers. The other surface parameters above are shown also to correlate for some types of fibers, but not as well for others. The results suggest that better correlations of surface morphology with ILSS might be obtained by examining the surface at dimensional scales below 25 nm. In general, it is felt that the ILSS

be enhanced by increasing surface roughness to provide not only greater mechanical interlocking, but also greater dipolar bonding with the matrix through polar moieties attached to the basal plane edges exposed by roughness.

Keywords: AFM; carbon fiber; composite; PMR-15; interlaminar shear strength

1. INTRODUCTION

Carbon fibers are important materials for advanced composites. They find wide applications in aerospace, recreational, and transportation markets because of their high specific strengths and moduli. The mechanical and physico-chemical properties of the fibers depend on the type of the precursor, manufacturing conditions, subsequent processing methods and other factors [1-3]. The structure is fairly well documented [2-4]. With a polymer matrix, such as polyimides, carbon-fiber reinforced composites are suitable for applications for which strength, stiffness, light weight, high temperature resistance, chemical inertness, and good fatigue characteristics are required [4].

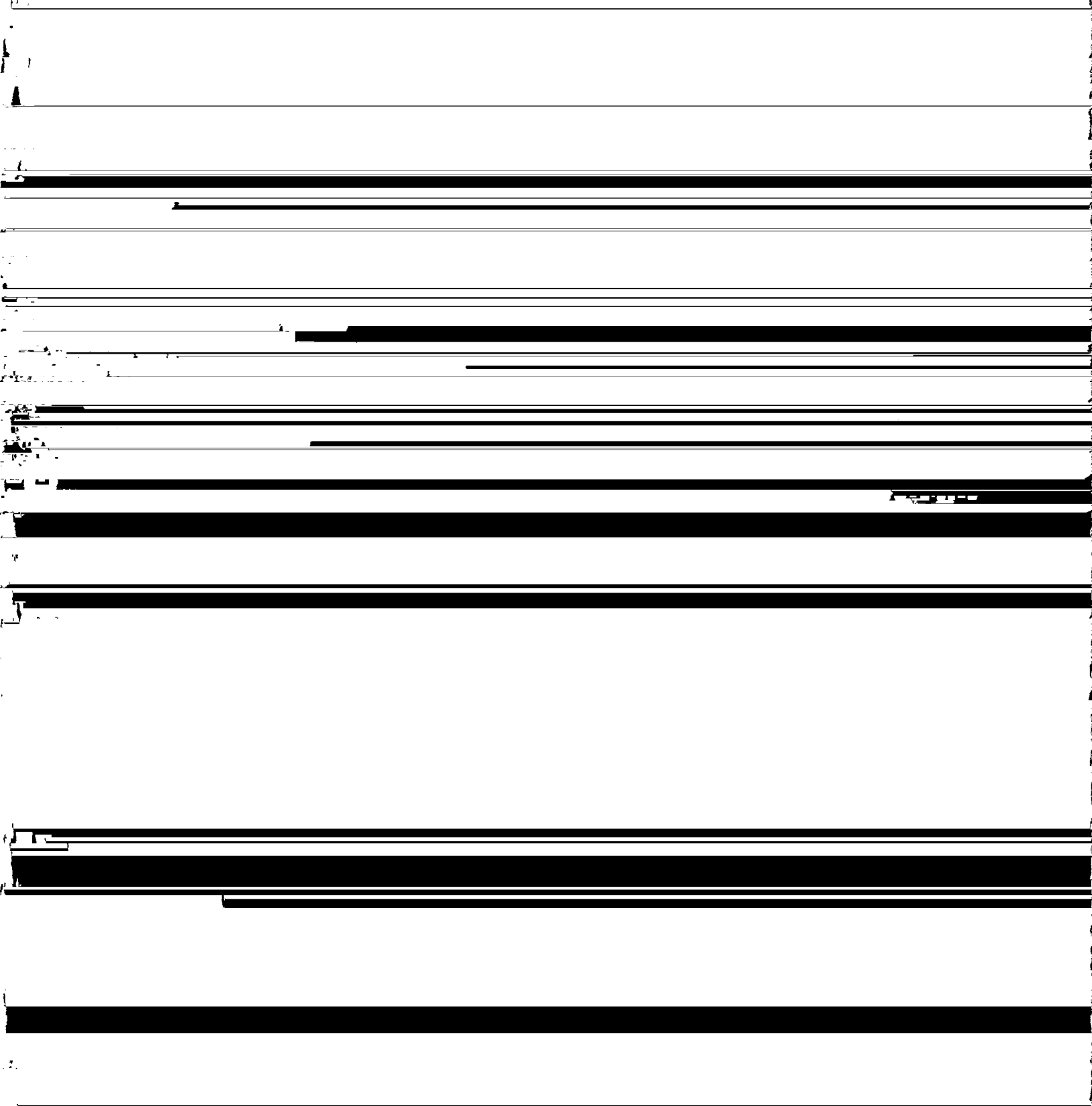
Advanced composites have been used increasingly in applications requiring the properties mentioned above [5]. Properties of the composites depend not only on the properties of the fibers and bulk matrix, but also on interfacial adhesion between them. The strength of adhesion at interfaces is determined by the types and degree of bonding between the fiber and the matrix. Possible mechanisms of carbon fiber-polymer matrix adhesion are believed to be: (a) covalent bonding, (b) dipole-dipole interaction, (c) dispersive interaction, and (d) mechanical interlocking [6]. The interfacial adhesion is expected to depend considerably on the quality and functionality of the fiber surface as well as the chemistry of the polymer matrix which helps to determine the first three mechanisms. The surface roughness as well as porosity of the fiber also can affect the degree of mechanical interlocking.

The interfacial interactions between the fiber and the matrix are not completely understood. For example, one type of carbon fiber can exhibit better thermo-oxidative stability at high temperatures than another, but the stability can be reversed when they are incorporated in a polyimide matrix [7]. A better understanding of the fiber-matrix interactions is crucial for the provision of a basis for interface tailoring to enhance the performance of the advanced composites.

Scanning probe microscopy began to be developed with the invention of the scanning tunneling microscope (STM) in 1982 [8]. Its success has led to the invention of a host of other scanning probe microscopes, which rely on mechanically scanning a sensing tip over a sample surface. The atomic force microscope (AFM), also known as the scanning force microscope is one of the most successful of these new devices [9]. Both STM and AFM offer great promise for the investigation of surfaces to the atomic level which has not been readily accessible by other techniques. However, AFM has more general applicability because electrical conductivity of the investigated sample is an important requirement for STM, but is not necessary for AFM. The AFM provides three-dimensional data on surface topography. The digitized image data can be analyzed readily by surface analysis software to obtain surface parameters, such as, average surface roughness (R_a), surface area (A_c), fractal dimension (F_d), etc.

In this work, the AFM is used to investigate the surface topography of various commercially available PAN-based fibers in order to gain a better understanding of the bonding mechanisms involved in carbon fiber/PMR-15 composites. The present research is focused on extending our previous work [1, 10, 11]. It has been shown that the polar component on the fiber surfaces

(characterized as percent weighted dipole moment - % WDM and % polar energy) is completed



fibers were mounted on sample holder disks with a thermoplastic adhesive, Tempfix[®] (Structure Probe, Inc.). Laminates were fabricated according to a process described elsewhere [12]. Specimens for isothermal aging were taken from void-free portions.

2.2. Methods

2.2.1. *Atomic force microscopy (AFM)*. A commercial AFM, TopoMetrix[®] TMX-2000 (TopoMetrix Inc., Santa Clara, California, USA), was used at ambient conditions to image the surface topography. The probe stage was mounted on a home-made anti-vibration platform comprising a heavy stone hung from bungee cords in order to reduce unwanted motions of the tip relative to the sample. Tips with a high aspect ratio of 10 to 1 and a radius of 10 nm were used. The geometry of the probe tips is especially important to the quality of the AFM images on a rough surface [10]. A ten μm scanner was used in the constant force mode on the 1-5 μm observation scale, and a one μm scanner was used in the variable force mode for scanning high resolution images. The line scan rate was set to be 3 Hz to collect 200 x 200 data points per image. To minimize sample damage, the force used at the cantilever was set very low (in the range of 10^{-10}N).

2.2.2 Isothermal Aging

Forced air convection ovens were used for long-term exposure at 316° C. Weight loss measurements were made on samples removed from the ovens after various time intervals throughout the exposure periods. Interlaminar shear strength tests were performed according to

ASTMD-2344. End cross sections were polished in the metallographic style and imaged in a Cambridge Stereascan 200 scanning electron microscope (SEM).

3. RESULTS AND DISCUSSION

3.1 Thermo-oxidative aging

Figure 1 shows the ILSS and Fig. 2 the weight loss as a function of % WDM and extended aging time to 1200 hours. Fibers with a higher % WDM exhibit a greater initial ILSS. Further, those with a higher % WDM lose both mass and ILSS more slowly with time. More importantly, these two effects appear to be interrelated. Figure 3 shows typical electron micrographs of cross sections of the AU4 and AS 4 composites after 600 hours of aging. The former which has the lower % WDM has lost much of its ILSS and cracks have developed around the fibers. However, the AS4 composite which has a stronger interfacial bond has not yet lost so much of its bond strength and has developed fewer and smaller cracks. After 900 hours it has done both. Moreover, both composites qualitatively appear to lose mass more rapidly after the ILSS has dropped considerably (600 h for AU4 and 900 h for AS4). This is consistent with the possibility that after the interfacial bonds break (lowering the ILSS), oxygen can diffuse along the interface forming the cracks and increasing the rate of mass loss.

Figure 4 shows the relationship between % WDM and initial ILSS in more detail than does Fig. 1. The effect of increasing % WDM on ILSS is less at higher values than at lower ones suggesting the possibility of a limiting value of ILSS. Figure 5 is consistent with this possibility.

The graph of ILSS vs. Reciprocal % WDM is a straight line which extrapolates to a limiting value of about 170 Mpa. A possible explanation of this observation is that the increasing concentration of dipoles on the fiber surface saturates the possible interactions with the dipoles on the surrounding matrix. There are some possible complications to be remembered. For example, there are hydroxyl, carbonyl and carboxyl polar groups on the fibers.[1] As the % WDM increases in Figs. 4 & 5, the relative amount of each is changing.[1,13] Thus, a changing % WDM which is a single variable in Figs. 4 & 5 really involves a changing ratio of the concentration of three moieties each of which has a different dipole moment. Nevertheless, the results in Fig. 5 are encouraging. They certainly suggest a limiting value of ILSS. In turn, this suggests that, beyond some value of % WDM, it is necessary to increase the concentration of dipoles in the matrix to increase the ILSS.

3.2.1 AFM

To examine the question concerning the location of the exposed basal plane edges to which polar groups attach during surface treatment, previous AFM investigations [1] were extended to more fibers and more surface parameters. Figure 6 shows a typical image of an AU4 fiber. Extrusion marks running parallel to the fiber axis and particles from the fiber manufacturing process can be seen clearly in most of the images. The particles are not expected to be airborne impurities or contamination deposited after manufacturing. They are firmly embedded in the fiber surface. The number of particles found in each type of fiber decreases as the strength of the fiber examined increases. This might be expected since impurity particles on and in PAN-based fibers are the main source of "flaws" limiting the strengths of the fibers [2]. As the magnification was

increased, grain-type structures of different sizes and shapes were found. A typical variable force image revealing grains on the surface of an AS4 fiber is shown in Fig. 7. Note that the grooves between grains are shallow and difficult to observe in constant force images. The grains are similar to those observed on T300, G40-600, G40-800 and M40 PAN-based fibers [10, 14].

3.2.2 Surface Characterization

The average roughness (R_a) can be defined as the arithmetic mean of the absolute values of departures of the roughness profile from the mean height of the surface with respect to a reference value. The roughness was determined for square scanning areas of 4, 9, and 25 μm^2 . For each size, images of eight randomly selected areas were obtained. In order to reduce the effect of the curved surface of the fiber on the roughness measurement, each image was "flattened" by fitting a second order equation to the height of the image and subtracting it from the digitized data [15]. Six scan lines perpendicular to the fiber axis were selected randomly for each image and used to analyze the roughness. As expected, the larger scanning areas had greater apparent roughness because the second order flattening did not completely remove the effects of curvature. Further, the fibers were not perfectly circular. Therefore, extrapolations of the plots of surface roughness vs scanning area to zero scanning area were performed in order to eliminate the effect of residual curvature [1]. Note that the lateral extent of the smallest scanning area was larger than that of the largest observed roughness features. An extrapolation of the roughness for the G40-800 fiber is shown in Fig. 8. The images of additional scanned areas were taken and analyzed to determine that the extrapolation was better performed vs the scanned area than the scanned length. The results in Fig. 9 show that the roughness of the fibers no longer correlates linearly with % WDM

for all the fibers, and, therefore, with the ILSS. There are a number of possible reasons for this result.

For example, the correlation might be complicated by the effects of other bonding mechanisms. Thus, roughness could contribute to mechanical interlocking as well as expose sites for the attachment of dipoles. However, attempts to fit the ILSS values to a quadratic in % WDM and R_a did not resolve the question. The fit was unsatisfactory. Another possibility is that a different characterization of surface topology might be required. One can imagine that R_a might not correlate well with the % WDM and ILSS since it does not differentiate between a variety of feature sizes on the surface. For example, two surfaces might have the same average amplitude of roughness, but one could have roughness of a short lateral extent or "wavelength" and the other a long one. Even though the two surfaces have the same value of R_a , these different morphologies might expose different amounts of surface area and basal plane edges. Such a difference might exist between the G/T fibers and the A fibers. Therefore, surface area was considered. It can be calculated approximately by transforming the digitized AFM data into x, y, and z coordinations, and calculating the area as the cross product between two vectors, u and v, connecting sequential points of the image in the two directions of the scanning grid. [16]

$$Area = |u \times v| = \Delta x \Delta y \sqrt{(\partial z / \partial x)^2 + (\partial z / \partial y)^2} \quad (1)$$

Here Δx and Δy are the horizontal step sizes in the grid directions. Note that the area calculated by the opposite ends of the grid might not be equal, so the reported area is the average of both calculated values which differed little. In order to normalize the areas of the fibers, an "ideal"

or basal area, defined by the lateral and longitudinal displacements of the scanner was determined. The calculated areas were then reduced by this area and divided by it for normalization. The result is reported as "normalized excess surface area". As for R_a , the normalized excess areas of 4, 9, and 25 μm^2 scans were calculated and extrapolated to zero scanning area to eliminate the curvature effect. The plot of normalized excess surface area vs % WDM is shown in Fig. 10. Again, there is reasonable correlation for the G and T fibers, but the A fibers deviate to an unsatisfactory extent.

Another method of characterizing a surface is by fractal analysis. It permits a more detailed analysis of the roughness spectrum than most conventional roughness parameters which, in many cases, characterize a complex surface roughness by one number [17]. Fractal analysis characterizes a line profile by a number which can vary from one to two with one corresponding to a straight line and non-integral values greater than one corresponding to a line with a fractal roughness [18]. Further, this analysis of the roughness can be carried out on different dimensional scales and the results have been shown to be directly correlated with observable phenomena such as cleanability, corrosion, and adsorption [17,19,20]. In this work, the fractal dimension of lines across the images were determined via the "box counting" method [15]. The roughness profile is covered by a set of "boxes" and a count is made of the boxes that contain the profile. The slope of the curve of log box size vs log counts is the fractal dimension (F_d). The plot is often referred to as the "Richardson Plot" which gives F_d as a function of feature (box) size. The analysis was carried out for box sizes in 100 nm increments from 200 to 500 nm for the 25 μm^2 images. The analysis was carried out for box sizes of 25-50 nm and then in 50 nm

increments from 50 to 300 nm for the $4 \mu\text{m}^2$ images. As expected, the F_d increases as the feature size increases. However, the fractal dimensions of all the fibers are similar and exhibit little, if any, correlation with % WDM. These results suggest that if there is a correlation of F_d with % WDM it lies at a dimensional scale less than 25 nm.

4. CONCLUSION

Dipole interactions govern the ILSS and the thermo-oxidative stability of PMR-15/carbon fiber composites. The correlation between the inverse of the % WDM of the surface and the initial ILSS linear indicating a limiting value of the ILSS of about 170 MPa. Further increases of the ILSS require an increase of the polar components in the matrix. It is expected that the dipolar moieties are bonded to the surface at the exposed edges of the basal planes of the carbon crystals. However, a variety of surface characterization parameters (roughness, fractional excess surface area and fractal dimensions) do not correlate well with the % WDM. The results suggest that to identify the sites for bonding of the dipoles, the surface of the fibers should be examined at a smaller dimensional scale than about 25 nm. To do this on the rough fiber surface requires the use of the higher resolution of STM.

4. ACKNOWLEDGMENTS:

This work was supported by a grant and a Graduate Student Fellowship from the NASA Lewis Research Center. It also was supported by the NSF/EPIC Center for Molecular and

Microstructure of Composites. Part of the work was done by R.K. Eby while at the Max Planck Institut für Polymerforschung, Mainz, Germany on an Alexander von Humboldt Senior Award.

5. REFERENCES

1. A.M. Serrano, I. Jangchud, R.K. Eby, K.J. Bowles, and D.T. Jayne, in "High Performance Polymers and Polymer Matrix Composites", MRS Symposium Proceedings, Vol.305, (1993) p. 105
2. A.A. Konkin, in "Handbook of Composites, Volume 1 : Strong Fibres", W. Watt and B.V. Perov, Eds., Elsevier Science, New York (1985) p. 241
3. D. Hull, "An Introduction to Composite Materials", Cambridge University Press, Cambridge (1981) p. 9
4. J.-B. Donnet and R.C. Bansal, "Carbon Fibers", Marcel Dekker, Inc., New York (1984) p.78
5. M.A. Meador, in "Proceedings of the 2nd Annual HITEMP Review", NASA Conference Publication 10039 (1989) p.10-1
6. A.J. Kinloch, "Adhesion and Adhesives Science and Technology", Chapman and Hall, London (1987) p.56
7. K.J. Bowles, *SAMPE Quarterly* July, 6 (1990)
8. G. Binnig, H. Rohrer, Ch. Gerber, and E. Weibel, *Phys. Rev. Lett.* **49**, 57 (1982); see also G. Binnig, H. Rohrer, *Helv. Phys. Acta.* **55**, 726 (1982).
9. G. Binnig, C.F. Quate, and Ch. Gerber, *Phys. Rev. Lett.* **56**, 930 (1986)
10. I. Jangchud, *Master Thesis*, The University of Akron, Ohio (1992)

11. I. Jangchud, A.M. Serrano, R.K. Eby, P.E. Klunzinger, and M.A. Meador, in *Proceedings of the 21st Biennial Conference on Carbon*, ed. D.D.L. Chung, 197, American Carbon Society (1993).
12. K. Bowles and G. Nowak, *J. Compos. Mater.* **22**, 966 (1988)
13. A.M. Serrano, *Ph.D. Dissertation*, The University of Akron, Ohio (1994.)
14. S.N. Magonov, A.Y. Gorenberg, and H.-J. Cantow, *Polym. Bull.* **28**, 577 (1992)
15. "TopoMetrix TMX-2000 User Manual", TopoMetrix Corporation, Santa Clara (1992)
p.88
16. G.B. Thomas, Jr. and R.L. Finney, "Calculus and Analytic Geometry", 5th ed., Addison-Wesley, Ontario (1982)
17. B.B. Mandelbrot, "The fractal Geometry of Nature", Freeman, New York (1983)
18. S. Chesters, H.C. Wang, and G. Kasper, *Sol. Sta. Technol.* January, 73 (1991)
19. J.M. Gomez-Rodriguez and A.M. Baro, *J. Vac. Sci. Technol.* **B9**, 495 (1991)
20. J.M. Gomez-Rodriguez, A.M. Baro, L. Vazquez, R.C. Salvarezza, J.M. Vara, and A.J. Arvia, *J. Phys. Chem.* **96**, 347 (1992)

- Figure 1. ILSS of carbon fiber/PMR-15 composites after various thermo-oxidative exposures at 316° C. Each point represents the average of results for six specimens. Error bars of approximately ± 6 MPa for ILSS and ± 3 for % WDM are not shown.
- Figure 2. Weight Loss of carbon fiber/PMR-15 composites after various thermo-oxidative exposures at 316° C. Each point represents the average of results for four specimens. The error bars for Weight Loss lie within the symbols.
- Figure 3. End views of AU4/PMR-15 and AS4/PMR-15 composites after 600 hours of thermo-oxidative exposure at 316° C. The symbols F, P and C mark the carbon fibers, polymer matrix and cracks, respectively.
- Figure 4. ILSS of carbon fiber/PMR-15 composite as a function of % WDM.
- Figure 5. ILSS of carbon fiber/PMR-15 composite as a function of reciprocal % WDM.
- Figure 6. AFM constant force image of AU4 CF showing extrusion marks and dirt on a $2 \mu\text{m} \times 2 \mu\text{m}$ scanning area. The fiber axis is parallel to the extrusion marks.
- Figure 7. AFM variable force image of AS4 CF revealing grains on a $1 \mu\text{m} \times 1 \mu\text{m}$ scanning area. The fiber axis is parallel to the extrusion marks.
- Figure 8. Average roughness of G40-800 fibers as a function of scanning area.
- Figure 9. Average roughness at zero scanning area as a function of % WDM. The error bars represent the uncertainty of the intercept in the extrapolation to zero scanning area on graphs similar to the one in Figure 7. Scanning areas of 4, 9 and $25 \mu\text{m}^2$ were used for the extrapolation.
- Figure 10. Normalized excess surface area at zero scanning area as a function of % WDM.

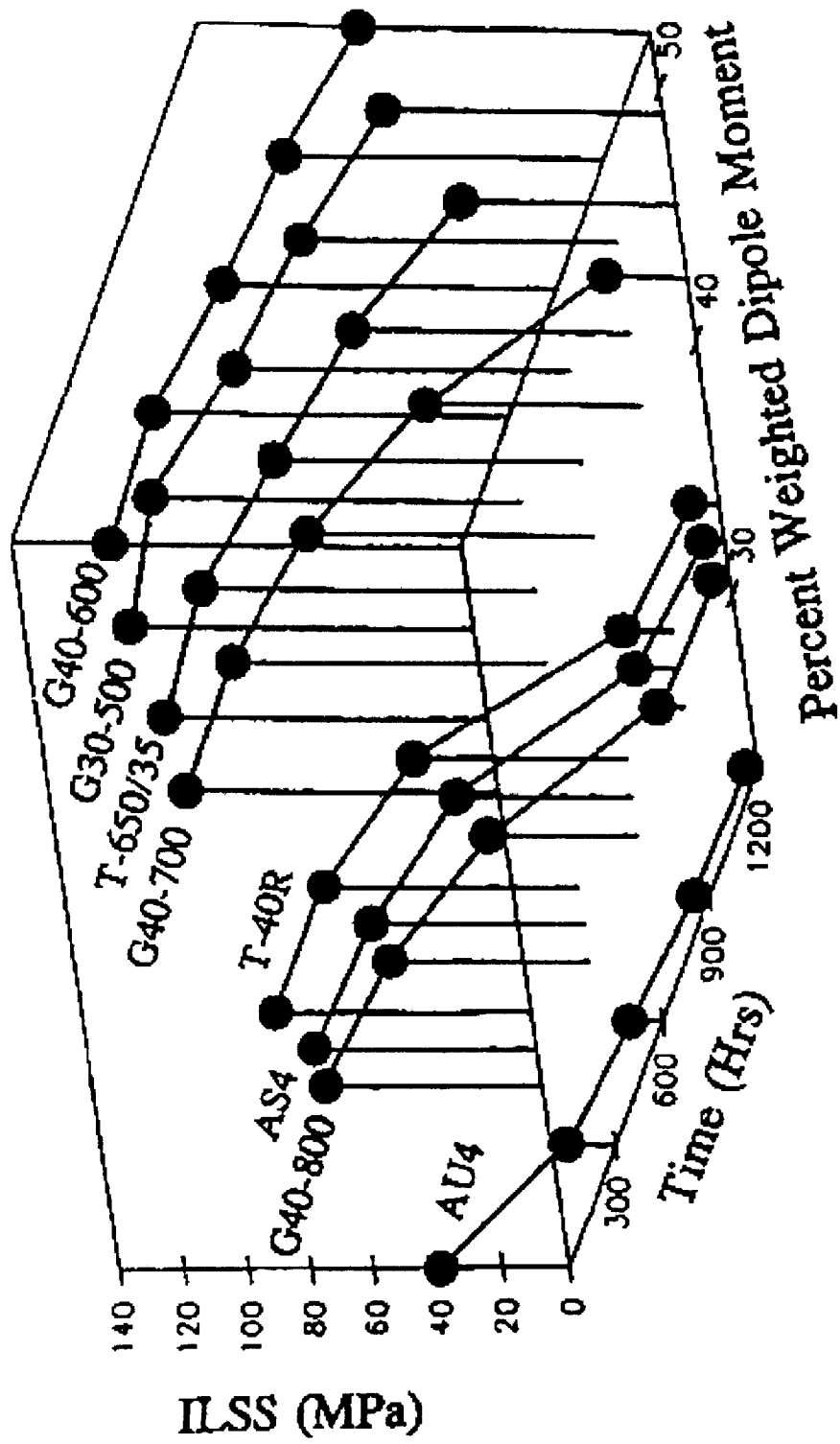


Figure 1

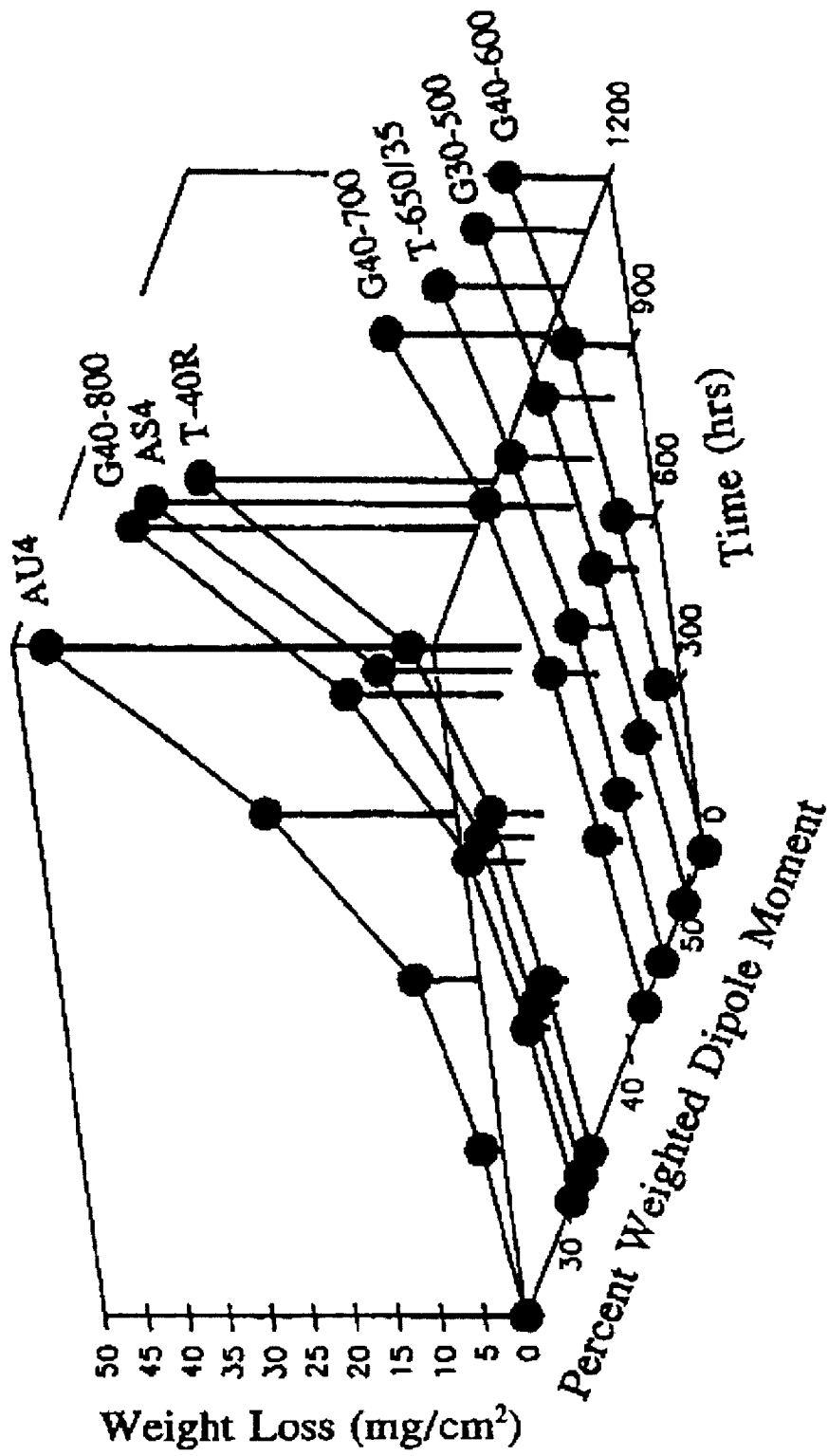


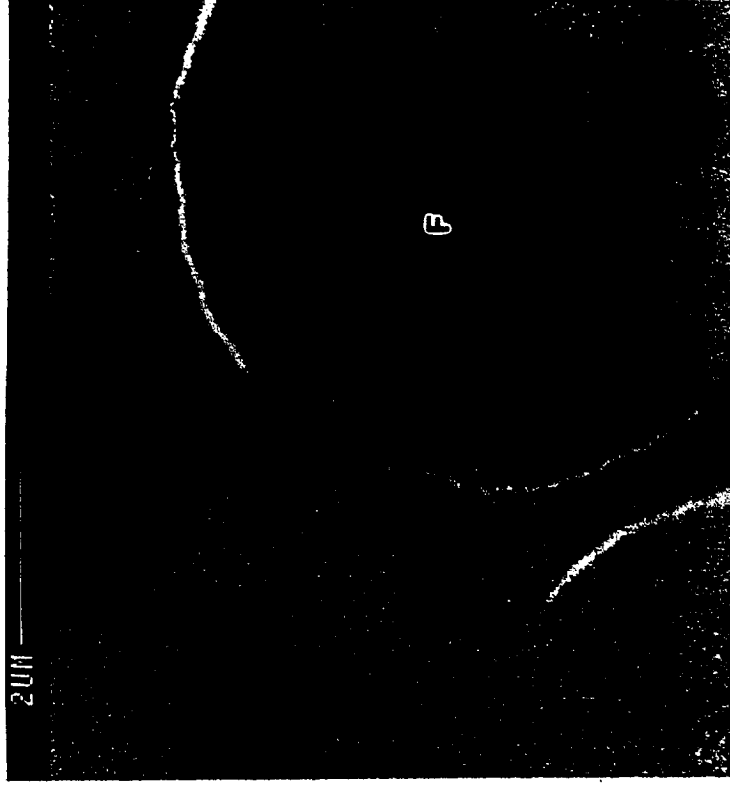
Figure 2

Figure 3

End Views of AU4/PMR-15 and AS4/PMR-15 Composites
After 600 Hours of Thermo-oxidative Exposure at 316°C.



AU4/PMR-15



AS4/PMR-15

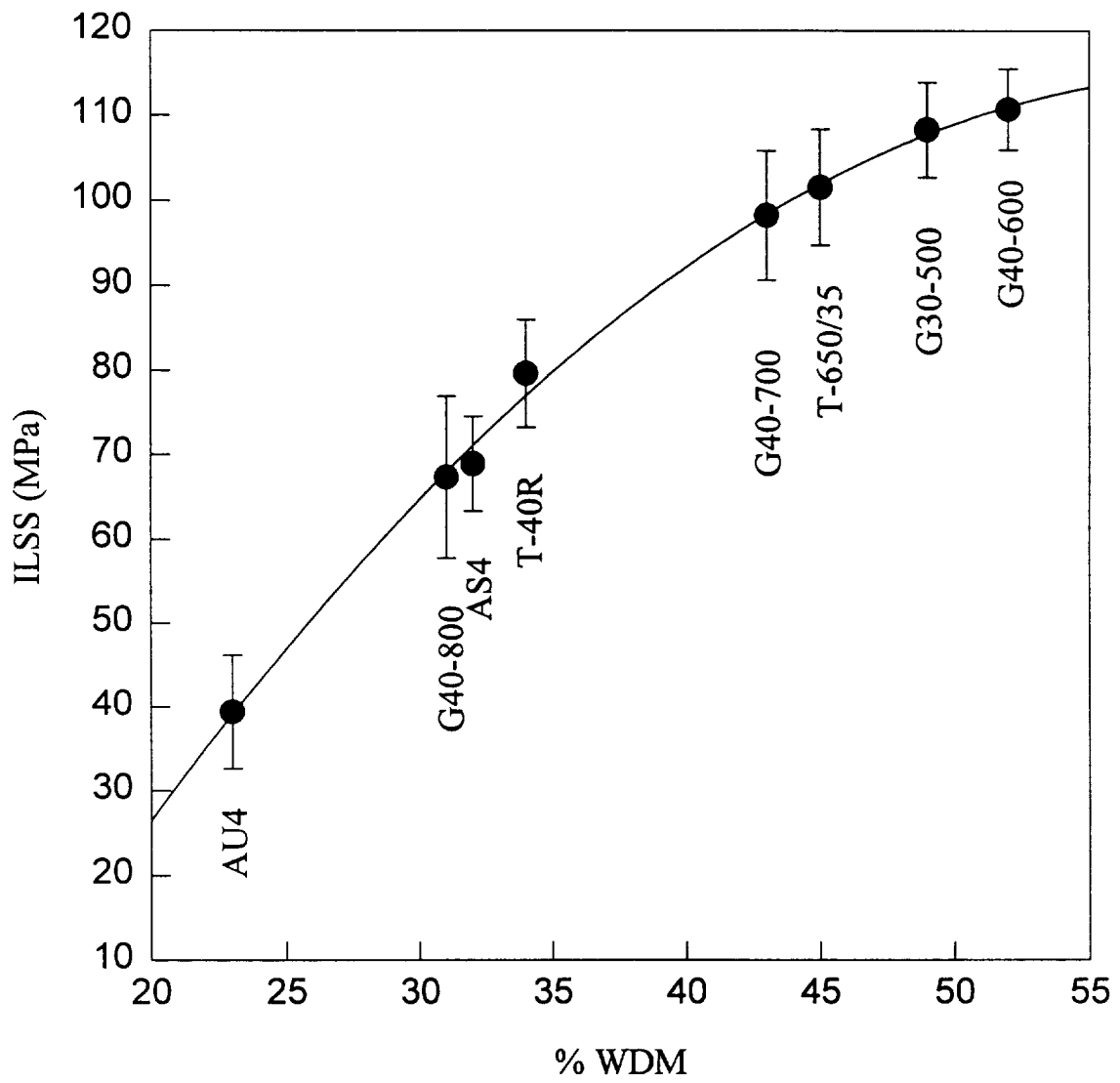


Figure 4

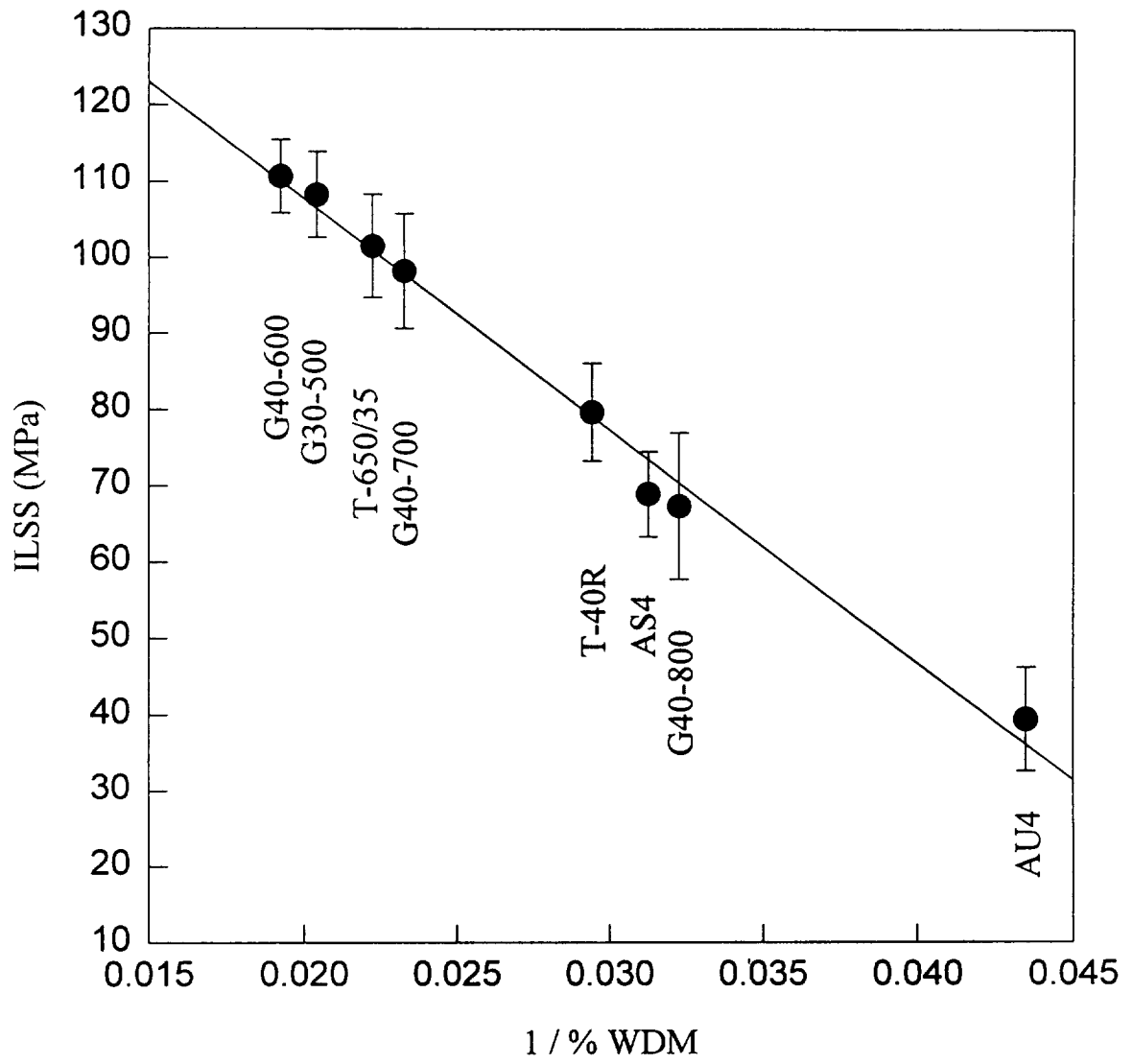


Figure 5

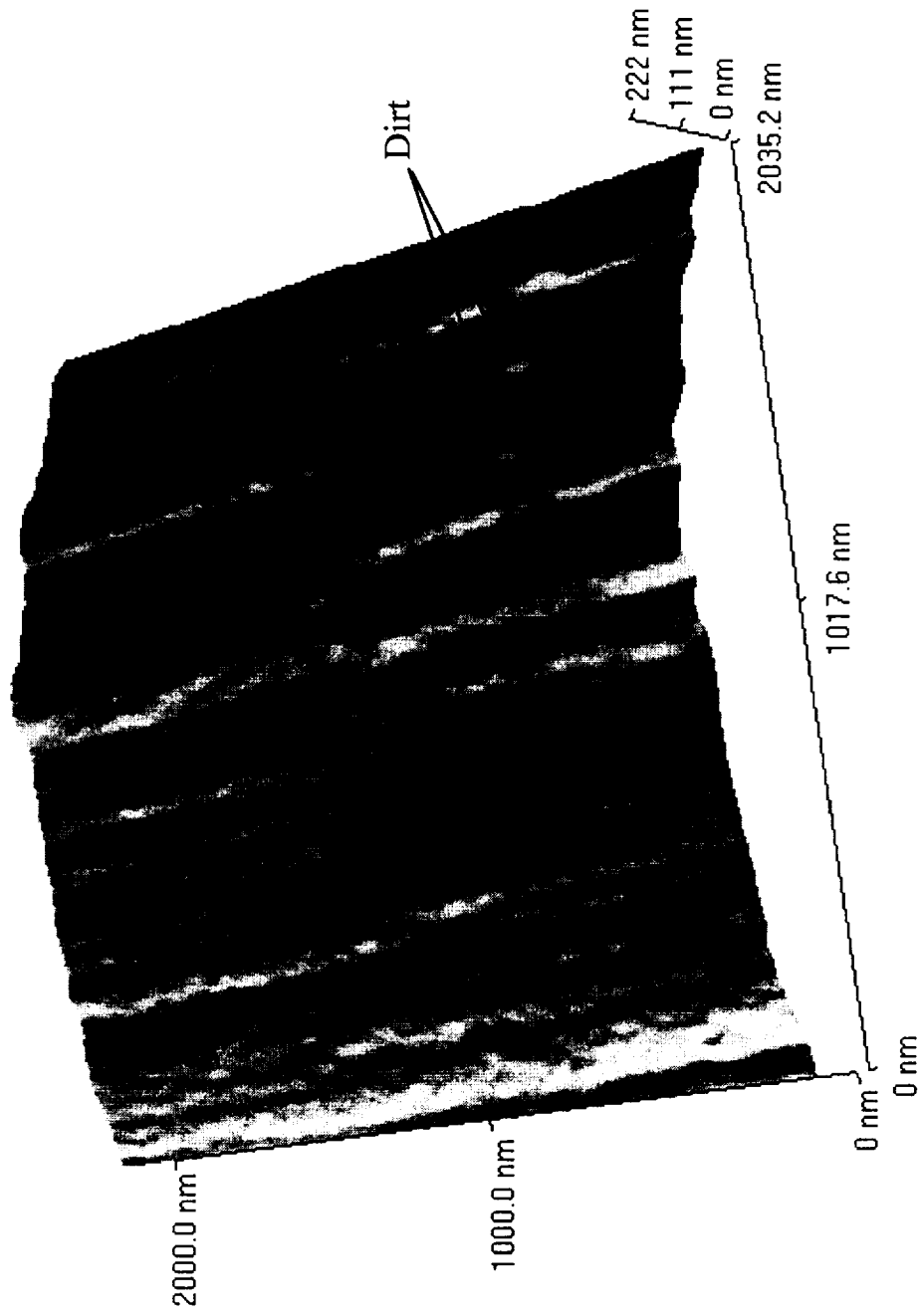
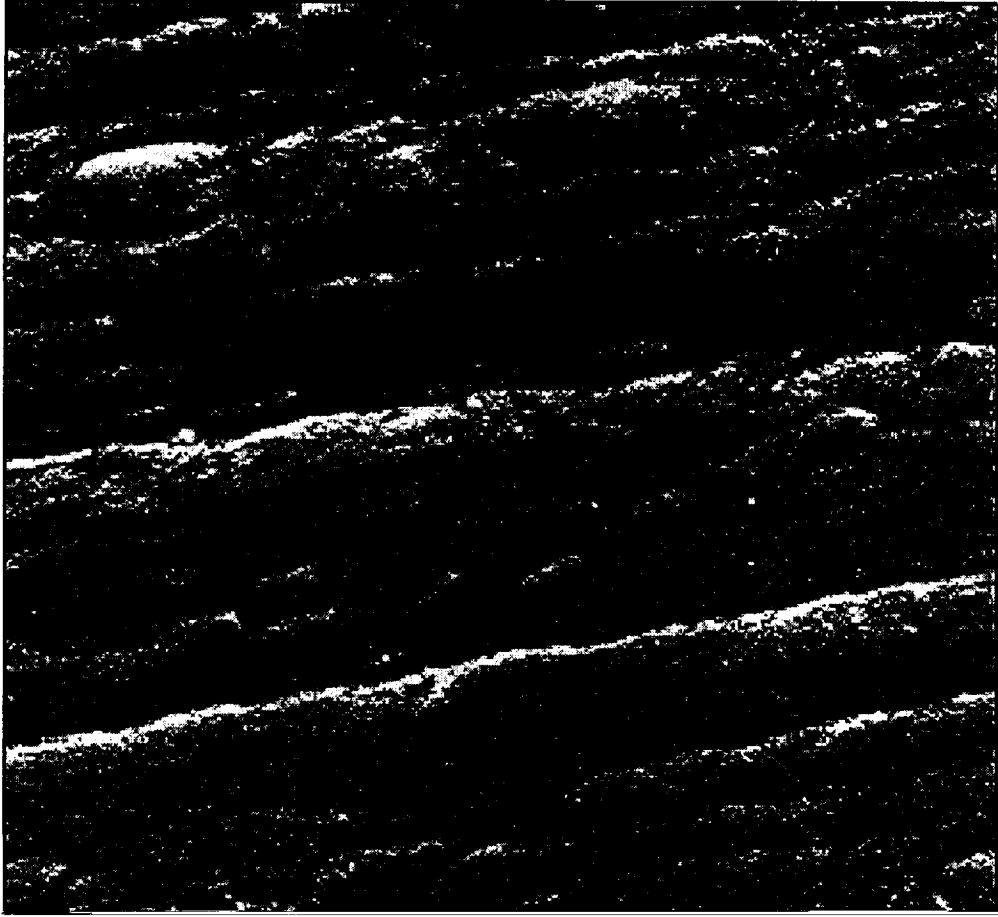


Figure 6



1000 nm

500 nm

Figure 7

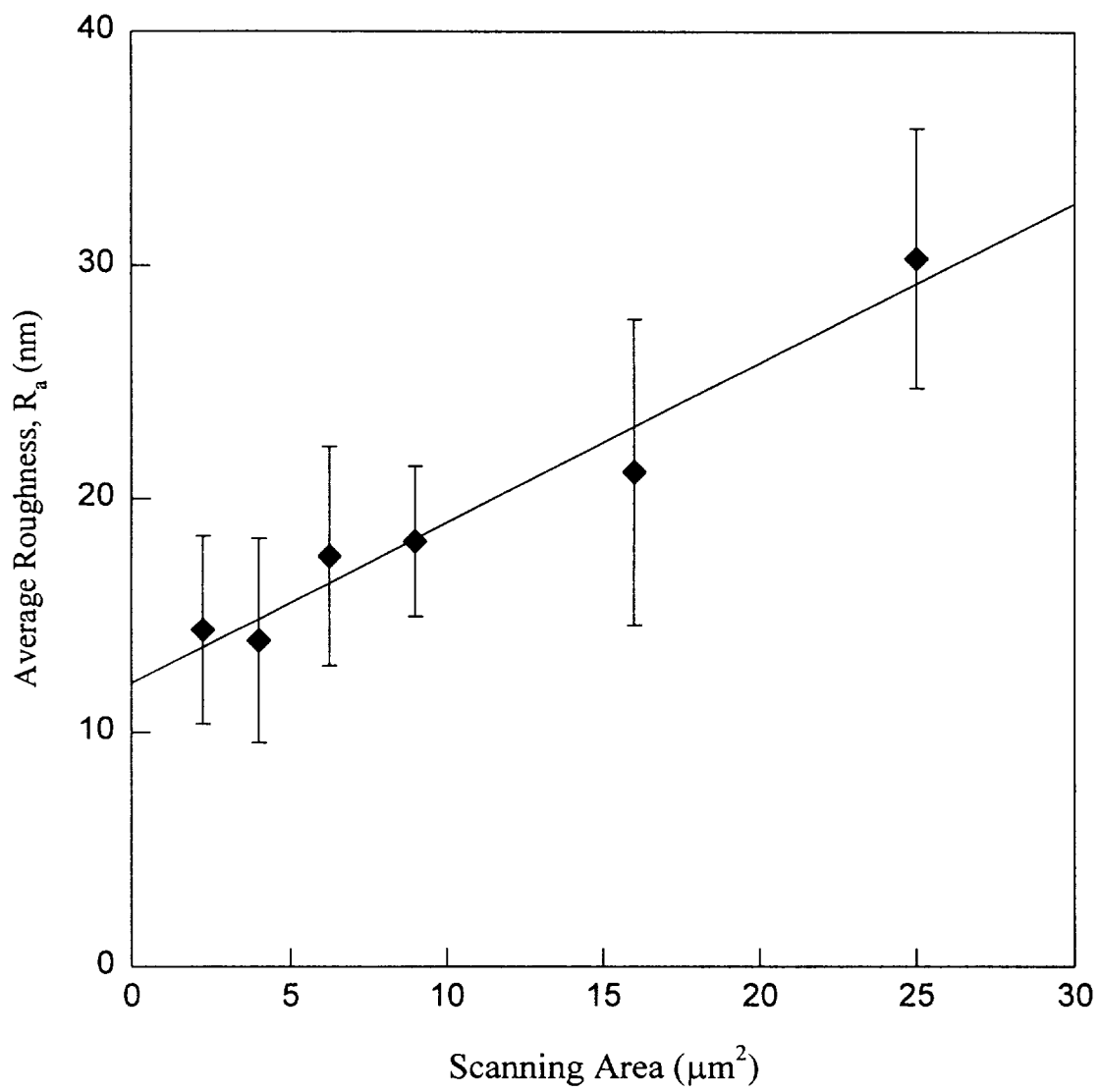


Figure 8

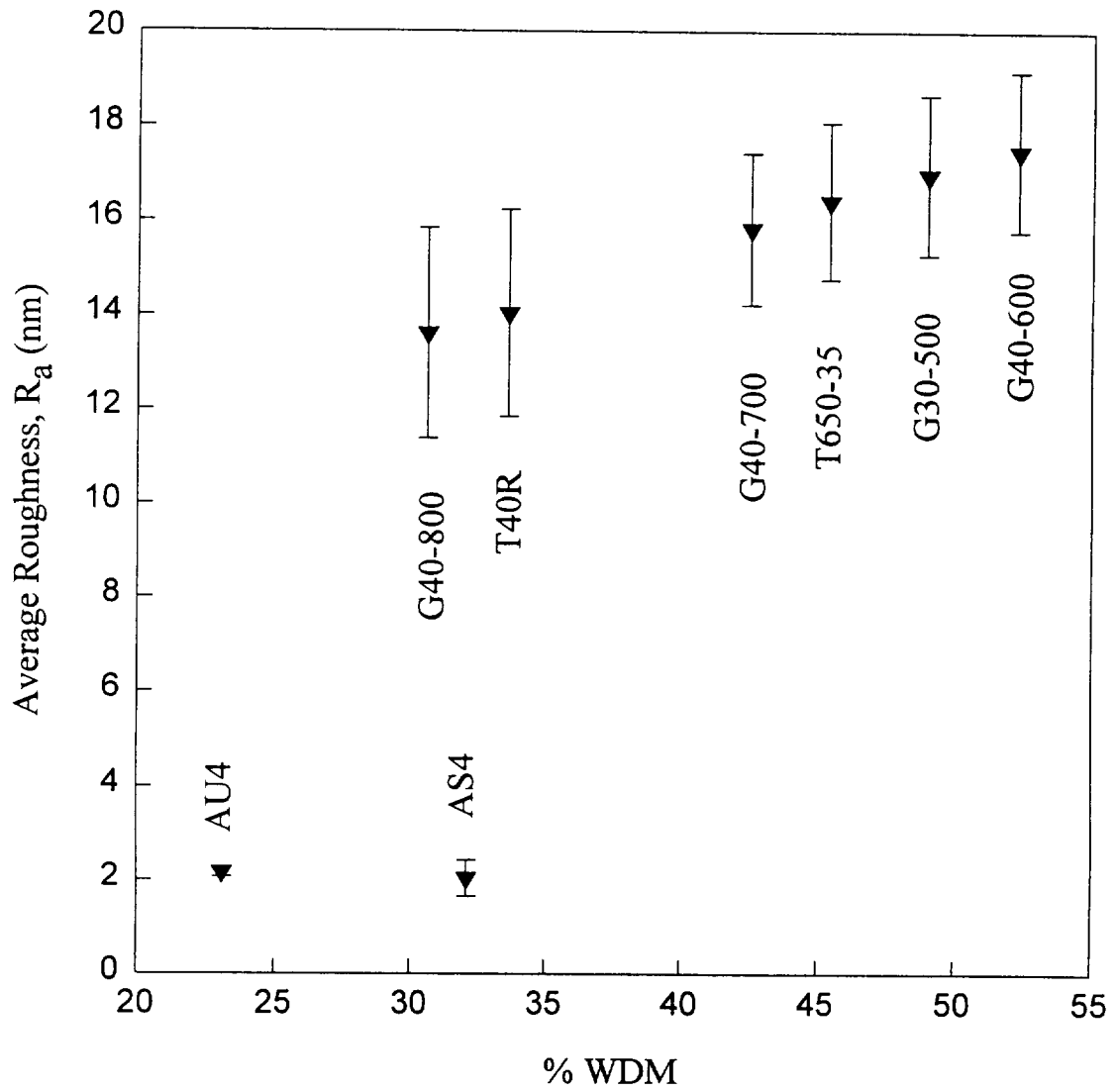


Figure 9

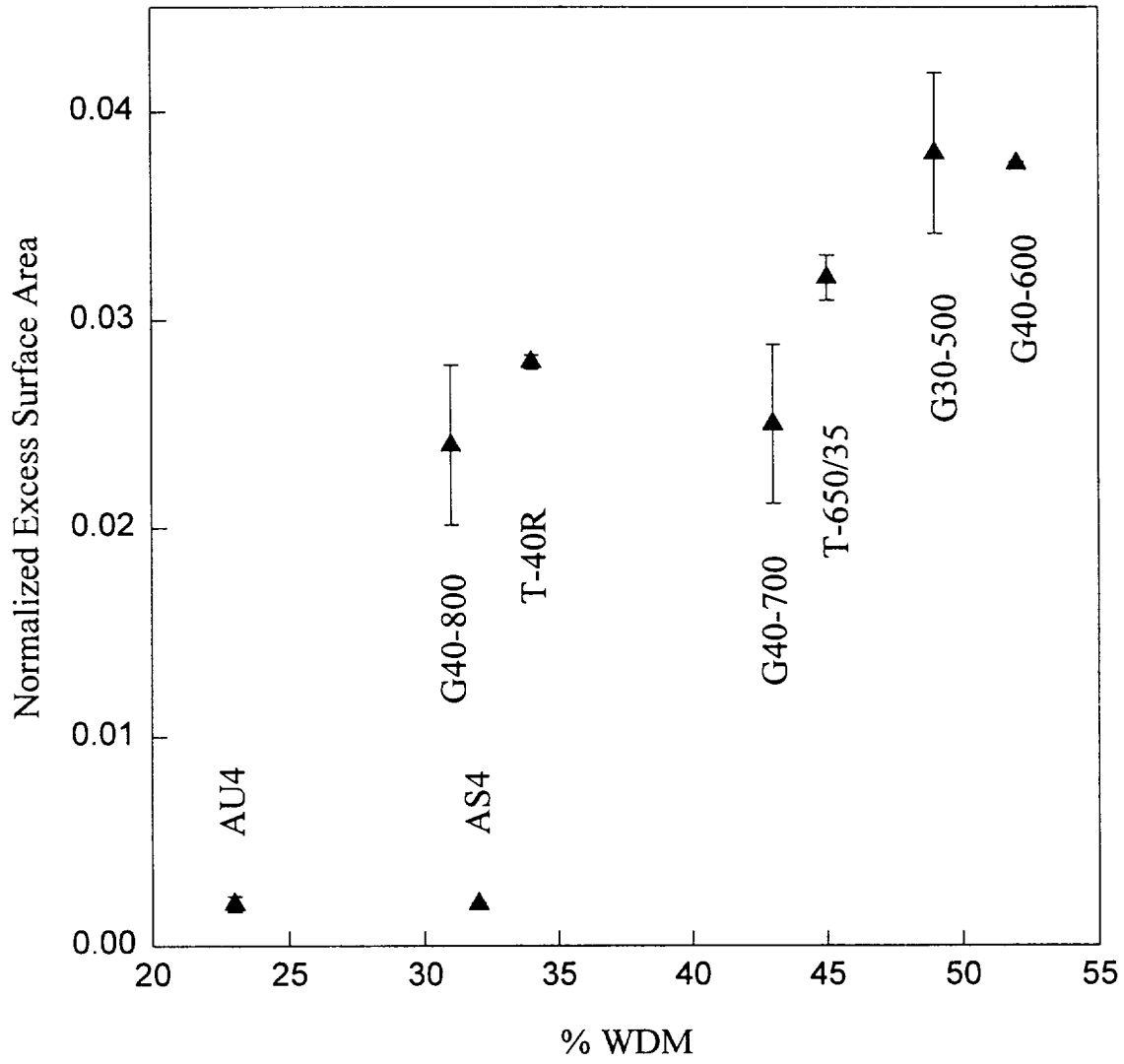


Figure 10